

## Synthesis, Characterization and Anti-Corrosion Properties of Novel Quinolinol on C-steel in a Molar Hydrochloric Acid Solution

M. Galai,<sup>a</sup> M. El Faydy,<sup>b</sup> Y. El Kacimi,<sup>a,\*</sup> K. Dahmani,<sup>c</sup> K. Alaoui,<sup>a</sup>  
R. Tourir,<sup>a,d</sup> B. Lakhrissi<sup>b</sup> and M. Ebn Touhami<sup>a</sup>

<sup>a</sup> *Laboratory of Materials Engineering and Environment: Modeling and Application, Faculty of Science, University Ibn Tofail BP. 133-14000, Kenitra, Morocco*

<sup>b</sup> *Laboratoire d'Agroressources et Génie des Procédés, Faculté des Sciences, Université Ibn Tofail, BP 133, Kénitra 14000, Morocco*

<sup>c</sup> *Laboratory of Materials, Electrochemistry and Environment, Faculty of Science, Ibn Tofail University, Kénitra, Morocco*

<sup>d</sup> *Centre Régional des Métiers de l'Éducation et de la Formation (CRMEF), Avenue Allal Al Fassi, Madinat Al Irfane, BP 6210 Rabat, Morocco*

Received October 18, 2016; accepted February 16, 2017

---

### Abstract

New quinoline, namely 5-(ethoxymethyl)-8-quinolinol (M-QN), has been synthesized and characterized by different spectral methods, such as <sup>1</sup>H NMR, <sup>13</sup>C NMR and IR spectra. Its inhibitive action against the corrosion of carbon steel in 1.0 M hydrochloric acid solution was investigated at different temperatures in the range from 25±2 to 55±2 °C by a series of known techniques, such as weight loss, open circuit potential (OCP), electrochemical impedance spectroscopy (EIS) and Tafel polarization measurements. The inhibition efficiencies obtained from all employed methods are in good agreement with each other. The obtained results show that M-QN-compound is a very good inhibitor with an efficiency of 97.7 % at 10<sup>-3</sup> M additive concentration in a 1.0 M HCl solution. The inhibition efficiency increased with an increase of the inhibitor's concentration. Changes in impedance parameters (R<sub>ct</sub> and C<sub>dl</sub>) were indicative of adsorption of the compound (M-QN) on the metal surface, leading to the formation of a protective film. Tafel polarization measurements showed that M-QN inhibitor is of a mixed type. The adsorption of the inhibitor on the surface of carbon steel in a 1.0 M HCl solution was found to obey Langmuir's adsorption isotherm. The kinetic and thermodynamic parameters for carbon steel corrosion and inhibitor adsorption, respectively, were determined and discussed. On the bases of thermodynamic adsorption parameters, comprehensive adsorption (physisorption and chemisorption) for the studied inhibitors on carbon steel surface was suggested.

**Keywords:** Corrosion inhibition, carbon steel, 5-(ethoxymethyl)-8-quinolinol, hydrochloric acidic medium, potentiodynamic polarization, EIS.

---

\* Corresponding author. E-mail address: elkacimiyounes@yahoo.fr

## Introduction

Mild steel has been widely used as a main construction material for piping works in various industries. It has found applications in downhole casing or tubing, flow lines and transmission or distribution pipelines in oil and gas industries [1-3]. Petroleum oil well acidization is an essential technique that is routinely used in oil and gas industries for the purpose of stimulating oil-well to ensure enhanced oil production [4,5]. This process, however, endangers the useful life of steel gadgets as a result of acid driven corrosion. In order to prevent this undesirable reaction, corrosion inhibitors are often added to the acid solution during acidification process [6-8].

These compounds inhibit corrosion by adsorbing onto a metallic surface using heteroatoms (e.g., N, O, S), polar functional groups (e.g., -OH, -NH<sub>2</sub>, -NO<sub>2</sub>, etc.), pi-electrons and aromatic rings as adsorption centers [9-11]. Inhibitors retard metal corrosion by adsorbing onto a metallic surface, and the process is influenced by some factors, which include molecular size of inhibitor, nature of substituents, inhibitor concentration, solution temperature and nature of test solution [8-11].

These compounds can form either a strong coordination bond with metal atom or a passive film on the surface [12]. The corrosion inhibition of a metal may involve either physisorption or chemisorption of the inhibitor onto the metal surface. Electrostatic attraction between the charged hydrophilic groups and the charged active centers on the metal surface leads to physisorption. Several authors have showed that most inhibitors were adsorbed onto the metal surface by displacing water molecules from the surface and forming a compact barrier film [13, 32, 33].

Perusal of literature reveals that many N-heterocyclic compounds such as pyrimidine derivatives [14], triazole derivatives [15], tetrazole derivatives [16], phenyltetrazole derivatives [17, 18], indole derivatives [19], pyridazine derivatives [20], and benzimidazole derivatives [21], to mention but a few, have been used for the corrosion inhibition of iron or steel in acidic media. The effectiveness of quinoxaline derivatives (N-heterocyclic compounds) as effective corrosion inhibitors for carbon steel in acid media has been reported [22-24].

Quinolines and their derivatives are important constituents of pharmacologically active synthetic compounds [26], including biological activities, such as DNA binding capabilities [26], antitumor [27] and DNA- intercalating carrier [28]. Several 8-aminoquinoline compounds, for instance, Primaquine, have been applied as chemotherapeutics for the treatment of malaria disease [30]. Recently, the first quinoline-based structure (GS-9137) with very strong antiretroviral activity for HIV treatment has been synthesized [30]. Although some quinoline derivatives have been reported as corrosion inhibitors for steel in sulphuric acid medium [31], no work, to the best of our knowledge, has been documented on the corrosion inhibition potentials of quinoline derivatives, namely, 5-(ethoxymethyl)-8-quinolinol (*M-QN*) on hydrochloric acid medium.

5-(ethoxymethyl)-8-Quinolinol was synthesized to be used as a corrosion inhibitor. The choice of this compound was based on the consideration that this

compound contains many  $\pi$ -electrons and heteroatoms, which induce greater adsorption of the inhibitor, compared to other organic compounds.

By considering the above mentioned remarks, the inhibition effect of 5-(ethoxymethyl)-8-quinolinol (*M-QN*) on the corrosion of carbon steel in a 1.0 M HCl solution was studied using electrochemical techniques and weight loss measurements. The effect of temperature on the corrosion behavior of carbon steel in a 1.0 M HCl, without and with *M-QN*, was investigated. In addition, adsorption of *M-QN* on a carbon steel surface was studied to examine basic information about the interaction between inhibitor and metal surface. Finally, to complete this study, the adsorption mechanism of *M-QN*—molecules was proposed and is discussed.

## Experimental study

### Weight loss measurements

The chemical composition of the used carbon steel sample is shown in Table 1. The specimen's surface was prepared by polishing with emery paper at different grit sizes (from 180 to 1200), rinsing with distilled water, degreasing with ethanol, and drying at hot air.

**Table 1.** Chemical composition of the used carbon steel.

Material	Composition, % by wt.											
	C	Si	Mn	Cr	Mo	Ni	Al	Cu	Co	V	W	Fe
Carbon steel	0.11	0.24	0.47	0.12	0.02	0.1	0.03	0.14	<0.0012	<0.003	0.06	Balance

The used carbon steels specimens have a rectangular form of 2.5 cm  $\times$  2.0 cm  $\times$  0.05 cm. The immersion time for weight loss was 6 h at 25 $\pm$ 2 °C, and it was determined according to Hmamou et al. [39]. After the immersion period, the specimens were cleaned according to ASTM G [31-34]. The aggressive solution of 1.0 M HCl was prepared by dilution of analytical grade 37 % HCl with distilled water. The molecular formula of the examined inhibitor is shown in Fig. 1.

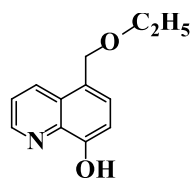


**Figure 1.** Chemical structure of 5-(ethoxymethyl)-8-quinolinol).

For every concentration, the mean value of the corrosion rate  $C_R$  (mg cm<sup>-2</sup> h<sup>-1</sup>) was determined, and the inhibition efficiency,  $\eta_{\omega}\%$ , was calculated using Eqs. (1) and (2), respectively:

$$C_R = \frac{W_b - W_a}{At} \quad (1)$$

$$\eta_{\omega} \% = \frac{\omega_{corr}^0 - \omega_{corr}}{\omega_{corr}^0} \times 100 \quad (2)$$

where  $W_b$  and  $W_a$  are the specimen weight before and after immersion in the tested solution,  $\omega_{corr}^0$  and  $\omega_{corr}$  are the corrosion weight losses of carbon steel in uninhibited and inhibited solutions, respectively,  $A$  the area of the carbon steel specimen ( $\text{cm}^2$ ), and  $t$  is the exposure time (h).

### Electrochemical measurements

For electrochemical measurements, the electrolysis cell was a borosilicate glass (Pyrex<sup>®</sup>) cylinder closed by a cap with five apertures. Three of them were used for the electrode insertions. The working electrode was pressure-fitted into a polytetrafluoroethylene holder (PTFE) exposing only  $1 \text{ cm}^2$  of area to the solution. Platinum and saturated calomel were used as counter and reference electrodes (SCE), respectively. All potentials were measured against the last electrode.

The potentiodynamic polarization curves were recorded by automatically changing the electrode potential from negative values to positive values versus  $E_{corr}$  using a Potentiostat/Galvanostat type PGZ 100, at a scan rate of  $1 \text{ mV s}^{-1}$  after 30 min immersion time until reaching steady state. The test solution was thermostatically controlled at  $25 \pm 2 \text{ }^\circ\text{C}$  in air atmosphere without bubbling. To evaluate corrosion kinetic parameters, a fitting by Stern-Geary equation was used. To do so, the overall current density values,  $i$ , were considered as the sum of two contributions, anodic and cathodic current,  $i_a$  and  $i_c$ , respectively. For the potential domain not too far from the open circuit potential, it may be considered that both processes followed the Tafel law [34]. Thus, it can be derived from equation (3) that:

$$i = i_a + i_c = i_{corr} \left\{ \exp[b_a \times (E - E_{corr})] - \exp[b_c \times (E - E_{corr})] \right\} \quad (3)$$

where  $i_{corr}$  is the corrosion current density ( $\text{A cm}^{-2}$ ) and  $b_a$  and  $b_c$  are the Tafel constants of anodic and cathodic reactions ( $\text{V}^{-1}$ ), respectively. These constants are linked to the Tafel slopes  $\beta$  ( $\text{V/dec}$ ) in a usual logarithmic scale given by equation (4):

$$\beta = \frac{\ln 10}{b} = \frac{2.303}{b} \quad (4)$$

The corrosion parameters were then evaluated by means of nonlinear least square method applying equation (2), using Origin software. However, for this calculation, the potential range applied was limited to  $\pm 0.100 \text{ V}$  around  $E_{corr}$ , because a significant systematic divergence was sometimes observed for both anodic and cathodic branches. The corrosion inhibition efficiency is evaluated from the corrosion current density values using the relationship (5):

$$\eta_{PP} = \frac{i_{corr}^0 - i_{corr}}{i_{corr}^0} \times 100 \quad (5)$$

The surface coverage values ( $\theta$ ) have been obtained from polarization curves for various concentrations of the inhibitor using the following equation (6):

$$\theta = 1 - \frac{i_{corr}}{i_{corr}^0} \quad (6)$$

where  $i_{corr}^0$  and  $i_{corr}$  are the corrosion current density values without and with inhibitor, respectively.

The electrochemical impedance spectroscopy measurements were carried out using a transfer function analyzer (VoltaLab PGZ 100), with a small amplitude a.c. signal (10 mV rms), over a frequency domain from 100 kHz to 100 mHz with five points per decade. The EIS diagrams were done in the Nyquist representation. The results were then analyzed in terms of an equivalent electrical circuit using Bouckamp program [36].

The inhibiting efficiency derived from EIS,  $\eta_{EIS}$ , was calculated using the following equation (7):

$$\eta_{EIS} = \frac{R_{ct} - R_{ct}^0}{R_{ct}} \times 100 \quad (7)$$

where  $R_{ct}^0$  and  $R_{ct}$  are the charge transfer resistance values in the absence and in the presence of the inhibitor, respectively.

In order to ensure reproducibility, all experiments were repeated three times. The evaluated inaccuracy did not exceed 10 %.

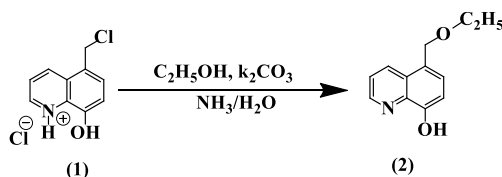


**Figure 2.** Mechanism of synthesis of 5-(ethoxymethyl)-8-quinolinol.

## Results and discussion

### Preparation and characterization of 5-(ethoxymethyl)-8-quinolinol (Fig. 2)

The melting points were determined on a digital automatic electrothermal IA 9200.  $^1\text{H}$  and  $^{13}\text{C}$  NMR spectra were recorded on a Bruker 300 WB spectrometer at 300 MHz, for solutions in Me<sub>2</sub>SO-*d*<sub>6</sub>. Chemical shifts are given as  $\delta$  values with reference to tetramethylsilane (TMS) as internal standard.

Infrared spectra were recorded from 400  $\text{cm}^{-1}$  to 4000  $\text{cm}^{-1}$  on a Bruker IFS 66v Fourier transform spectrometer using KBr pellets.

5-(chloromethyl)-8-quinolinol hydrochloride (1) was synthesized according to the method described by El Faydy et al. [37].

A mixture of 2.3 g, 0.01 mol of 5-(chloromethyl)-8-quinolinol hydrochloride (1), 25 mL of anhydrous ethanol and 0.84 g, 0.01 mol of added potassium bicarbonate ( $\text{K}_2\text{CO}_3$ ) was heated at reflux temperature for 1 hour. The mixture was poured into 50 mL of water and made alkaline with 5% of ammonium hydroxide. The product which precipitated was filtered, then dissolved in ether, and the ethereal solution was washed with water and dried over anhydrous sodium sulfate. After removal of the solvent, 5-ethoxymethyl-8-hydroxyquinoline (2) was crystallized from ethanol; yield 1.63g (80%); m.p.78-80 °C.

The FTIR spectra of 5-(ethoxymethyl)-8-quinolinol was displayed in Fig. 3. It is observed that the absorption peaks between 3800  $\text{cm}^{-1}$  and 2700  $\text{cm}^{-1}$  corresponded to -OH, and bands around 3026  $\text{cm}^{-1}$  for aromatic C=C and C-H stretching are observable. Instead, the absorption peaks between 1275  $\text{cm}^{-1}$  and 1298  $\text{cm}^{-1}$  related to CN, and strong and large peaks (2850  $\text{cm}^{-1}$ , 2940  $\text{cm}^{-1}$  and 1450  $\text{cm}^{-1}$ ) took place in the spectrum of 5-(ethoxymethyl)-8-quinolinol corresponding to the presence of  $\text{CH}_2$ .

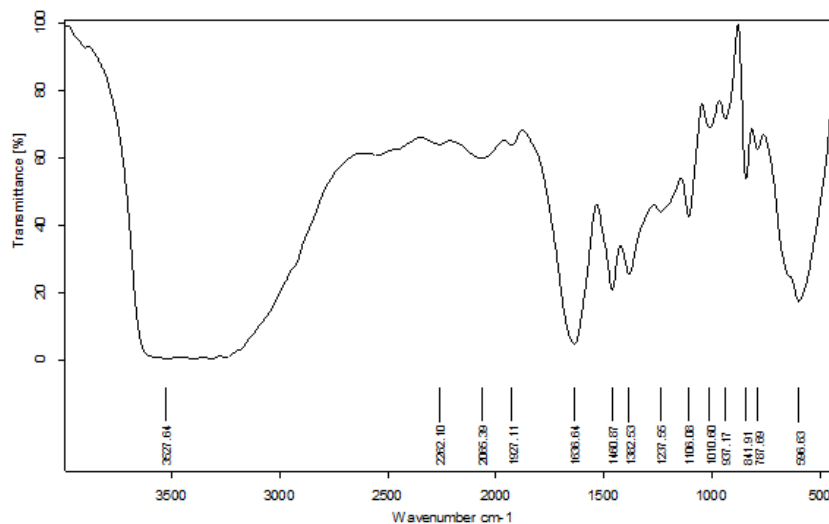
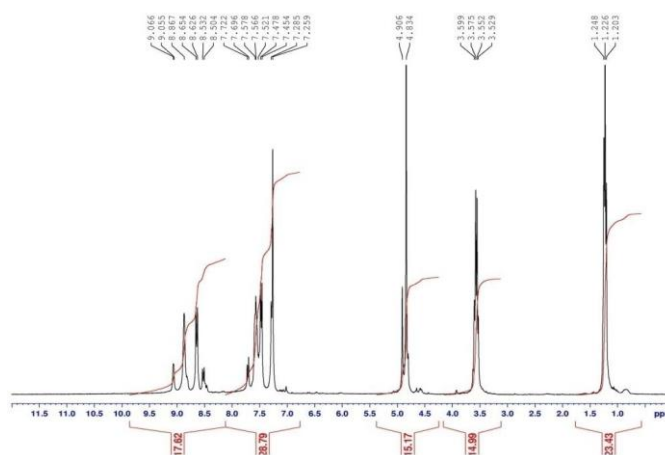


**Figure 3.** FTIR spectra of 5-(ethoxymethyl)-8-quinolinol.

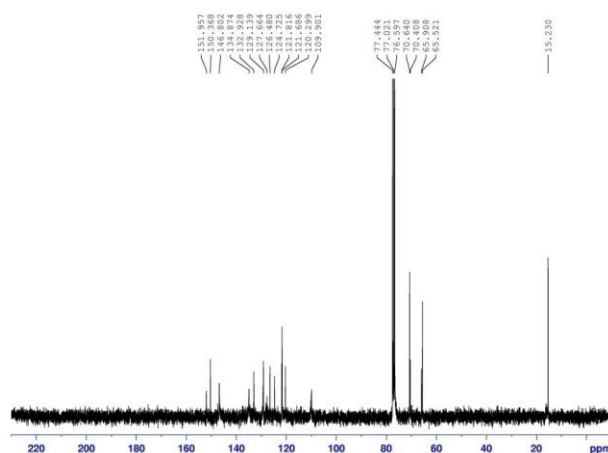
**Table 2.** Spectral data of the synthesized compounds.

Analytical technique	Spectral data	NMR spectra
$^1\text{H}$ NMR	(300 MHz, DMSO- $d_6$ ), $\delta_{\text{ppm}} = 7.037\text{-}9.066$ (m, 4H, quinoline), 4.906 (s, 1H, OH), 4.834 (s, 2H, aromatic- $\text{CH}_2\text{-O}$ ), 3.552 (m, 2H, O- $\text{CH}_2\text{-}$ ), 1.226 (m, 3H, - $\text{CH}_3$ )	Fig. 4
$^{13}\text{C}$ NMR	(75 MHz, DMSO- $d_6$ ), $\delta_{\text{ppm}} = 15.235, 65.908, 77.021, 109.901, 120.299, 126.480, 146.802, 150.368$	Fig. 5

$^1\text{H}$  and  $^{13}\text{C}$  NMR spectra were used to characterize and confirm the obtained product structure (see supplementary data) (Table 2).



**Figure 4.**  $^1\text{H}$  NMR spectra of 5-(ethoxymethyl)-8-quinolinol.

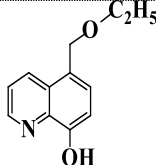


**Figure 5.**  $^{13}\text{C}$  NMR spectra of 5-(ethoxymethyl)-8-quinolinol.

### Weight loss measurements

The corrosion rate of carbon steel in 1.0 M HCl with and without different concentrations of M-Qn was determined after 6 h of immersion at  $25 \pm 2$  °C. This immersion time choice was made according to literature [39]. The obtained results are presented in Table 3. It has been observed that the corrosion rate ( $C_R$ ), decreases with an increase in inhibitor's concentration, M-Qn. At the same time, the inhibition efficiency,  $\eta_w$  (%), was enhanced by the inhibitor's concentration, reaching a maximum of 97.7% at  $10^{-3}$  M of M-Qn. The good inhibitive performance of 5-(ethoxymethyl)-8-quinolinol may be explained on the basis of adsorption of the molecule (physisorption and/or chemisorption). The M-Qn molecule can easily be protonated to form cation-ionic forms in an HCl solution, and therefore adsorb onto the metal surface through the already adsorbed chloride ions. Also, the adsorption of the neutral 5-(ethoxymethyl)-8-quinolinol molecule could occur through the formation of links between the d-orbital of iron atoms, involving the displacement of water molecules from the metal surface, the lone  $sp^2$  electron pairs present on the N, and O atoms and p-orbitals in the aromatic ring, blocking the active sites on the steel surface and, therefore, decreasing the corrosion rate. The inhibition efficiency increased with concentration of M-Qn, reaching a maximum at  $10^{-3}$  M of M-Qn. This behavior could be attributed to the increase in adsorption of the inhibitor at the metal/solution interface with the increase on its concentration.

**Table 3.** Corrosion rate and inhibition efficiency of carbon steel in 1.0 M HCl with different concentrations of M-Qn at  $25 \pm 2$  °C after 6 h of immersion.

Inhibitor	Conc. / M	$C_R$ / $\text{mg cm}^{-2} \text{h}^{-1}$	$\eta_w$ / %	$\theta$
Blank solution	00	49.07	-	-
	$10^{-6}$	3.1	93.7	0.9368
	$10^{-5}$	2.82	94.3	0.9425
	$10^{-4}$	2.53	94.8	0.9484
	$10^{-3}$	1.15	97.7	0.9766

### Open circuit potential (OCP) measurements

The variances of OCP of the carbon steel as a function of time in aerated 1.0 M HCl solution, in the absence and presence of different concentrations of M-Qn, are shown in Fig. 6.

Fig. 6 shows the differences of the open circuit potential (OCP), with time, for carbon steel corrosion against 1.0 M HCl solution in the presence and absence of M-Qn. It was noticed that the addition of the inhibitor molecule induces a continuous shift in OCP (i.e.,  $E_{\text{corr}}$ ) to nobler potentials, indicating the spontaneous adsorption of inhibitor onto the metallic surface.

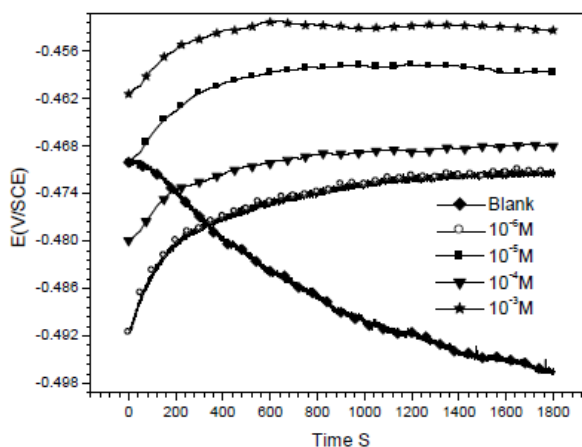


**Figure 6.** OCP vs. time during 30 min for carbon steel in 1.0 M HCl, and in the presence of different concentrations of M-Qn.

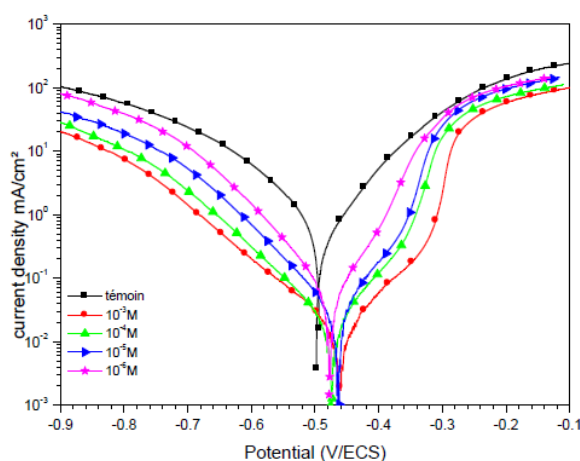


**Figure 7.** Potentiodynamic polarization curves for carbon steel in 1.0 M HCl without and with different concentrations of M-Qn.

Corrosion potential stabilization occurs after almost 600 (s) of immersion time in 1.0 M HCl solutions.

For  $10^{-3}$  M of M-Qn, OCP becomes more positive compared to  $10^{-6}$ ,  $10^{-5}$  and  $10^{-4}$  M of inhibitor. This means that the surface becomes nobler with an increased inhibitor concentration, which can probably be due to the stronger oxides formation on the metal surface. With the addition of  $10^{-3}$  M of M-Qn, the



presence of dissolved oxygen and  $H^+$  ions on metal surface is increased and can lead to formation of more oxides and more positive values of OCP [33].

### Potentiodynamic polarization curves

Potentiodynamic polarization curves of carbon steel in 1.0 M HCl without and with different concentrations of M-Qn at  $25 \pm 2$  °C are given in Fig. 7, and their extrapolation parameters and inhibition efficiencies are plotted in Table 4.

**Table 4.** Electrochemical parameters for carbon steel in 1.0 M HCl at various concentrations of M-Qn at  $25 \pm 2$  °C.

Conc. of M-Qn (M)	$-E_{\text{corr}}$ (mV/SCE)	$i_{\text{corr}}$ ( $\mu\text{A cm}^{-2}$ )	Tafel slopes ( $\text{mV dec}^{-1}$ )		$\eta_{\text{pp}}$ (%)
			$-\beta_{\text{c}}$	$\beta_{\text{a}}$	
00	-498	983	92	104	-
$10^{-6}$	-471	60	94	96	93.9
$10^{-5}$	-458	46	98	90	95.3
$10^{-4}$	-467	30	101	87	96.9
$10^{-3}$	-453	22	125	84	97.7

It can be seen that the M-Qn addition hindered the acid attack on carbon steel, and an increase in its concentration gave a decrease in anodic and cathodic current densities, indicating that this inhibitor acted as a mixed-type inhibitor. However, the cathodic Tafel slopes ( $\beta_{\text{c}}$ ) changed with the quinolinol substituted compound addition, indicating a modification of the mechanism of cathodic hydrogen evolution, which suggests that these compounds powerfully inhibit the corrosion process of carbon steel, and their ability as corrosion inhibitors are enhanced as their concentrations are increased. The suppression of the cathodic process can be due to the covering of the surface with a monolayer originated by the adsorbed inhibitor molecules [27]. It is also seen that the inhibition efficiency increased with concentrations, reaching a maximum of 97.7 % at  $10^{-3}$  M of M-Qn, and exhibited both cathodic and anodic inhibition through adsorption on carbon steel surface blocking active sites [28]. So, a slight definite change on the corrosion potential ( $E_{\text{corr}}$ ) was observed. According to Riggs [29] and other authors, if the displacement in  $E$  is  $> 85 \text{ mV} / E_{\text{corr}}$ , the inhibitor can be seen as of the cathodic or anodic type; if the displacement in  $E$  is  $< 85 \text{ mV} / E_{\text{corr}}$ , the inhibitor can be seen as of the mixed type. In our study, the maximum displacement is less than  $85 \text{ mV} / E_{\text{corr}}$ , which indicates that M-Qn is a mixed type inhibitor. The results obtained by the potentiodynamic polarization curves confirmed those obtained by weight loss measurements.

### Electrochemical Impedance Spectroscopy (EIS)

The aim of this section was to confirm the obtained results by potentiodynamic polarization curves and weight loss measurements. Fig. 8 presents the Nyquist plots of carbon steel in 1.0 M HCl, without and with different concentrations of M-Qn at the corrosion potential. It is noted that the Nyquist plot of carbon steel in the absence and presence of all concentrations of inhibitors contains a slightly depressed semi-circular shape, and only one time constant appeared, indicating that carbon steel corrosion is mainly controlled by a charge transfer process.

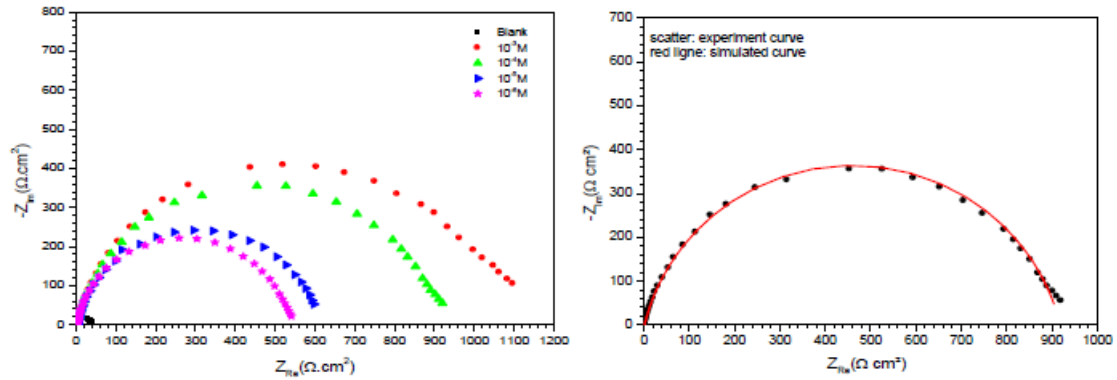


**Figure 8.** Nyquist plots for carbon steel in 1.0 M HCl solution in the absence and presence of various concentrations of M-Qn at  $E_{\text{corr}}$  ( $T=25\pm 2$  °C): comparison of experimental (scatter) and fitting (red line) data.

In this case, it can be seen that these plots were composed by one capacitive loop in the absence and presence of different concentrations of M-Qn. This behavior can be attributed to charge transfer of the corrosion process. It is also noted that the diameter of the semicircle increased with the inhibitor’s concentration, indicating an increase in corrosion resistance of the material [43].

However, a CPE element was employed in order to investigate the inhibitive film properties on the metallic surface. Thus, the impedance of CPE can be described by the following equation:

$$Z_{\text{CPE}} = [Q(j\omega)^n]^{-1} \quad (8)$$

where  $j$  is an imaginary number,  $Q$  is the frequency independent real constant,  $\omega = 2\pi f$  is the angular frequency ( $\text{rad s}^{-1}$ ),  $f$  is the frequency of the applied signal,  $n$  is the CPE exponent for whole number of  $n = 1, 0, -1$ , and CPE is reduced to the classical lump element-capacitor (C), resistance (R) and inductance (L) [44]. The use of these parameters, similar to the constant phase element (CPE), allowed the depressed feature of Nyquist plot to be readily reproduced.

In addition, the effective calculated double layer capacitance (C) derived from the CPE parameters according to the following equation [45]:

$$C = Q^n \times R^{\frac{1-n}{n}} \quad (9)$$

The most important data obtained from the equivalent circuit are presented in Table 4. It may be remarked that  $R_{\text{ct}}$  values increased, while  $C_{\text{dl}}$  values decreased with inhibitor’s concentrations, indicating that more inhibitor molecules are adsorbed onto the metallic surface, providing better surface coverage and/or enhancing the thickness of the protective layer at the metal/solution interface [46, 47]. In addition, these changes in  $R_{\text{ct}}$  and  $C_{\text{dl}}$  can be attributed to the gradual displacement of water molecules and/or chloride ions on the carbon steel surface [48], leading to a protective solid film, and then to a decrease in the extent of the dissolution reaction [49, 50]. In its turn, the decrease of  $C_{\text{dl}}$  with concentrations can be explained by the decrease in local dielectric constant and/or the increase in the protective layer thickness on the electrode surface. This trend is in accordance with Helmholtz model, given by the following equation [51]:

$$C_{dl} = \frac{\varepsilon_0 \times \varepsilon}{e} \times S \quad (10)$$

where  $\varepsilon$  is the dielectric constant of the protective layer,  $\varepsilon_0$  is the permittivity of free space ( $8.854 \times 10^{-14}$  F cm<sup>-1</sup>) and  $S$  is the effective surface area of the electrode. However, the inhibition efficiencies obtained from electrochemical impedance measurements increase with concentration and show the same trend as those obtained from potentiodynamic polarization and gravimetric measurements.

However, the results can be interpreted using the equivalent circuit presented in Fig. 9, which has been previously used to model the iron/steel interface [52].



**Figure 9.** Equivalent circuit used to model impedance data in 1.0 M HCl solutions in the presence of different concentrations of M-Qn.

Excellent fit with the model was obtained for all experimental data (Fig. 10). The Nyquist and Bode plots of both experimental and simulated data of carbon steel in 1.0 M HCl solution without and with  $10^{-3}$  M of M-Qn are shown in Fig. 11. It is clear that the impedance plots are in accordance with those calculated by the used equivalent circuit model. Various parameters such as charge-transfer resistance ( $R_{ct}$ ), double layer capacitance ( $C_{dl}$ ) and degree of heterogeneity ( $n_{dl}$ ) obtained from impedance measurements are shown in Table 5, which contains all the impedance parameters obtained from the simulation of experimental impedance data, including  $R_{ct}$  and  $n$ .

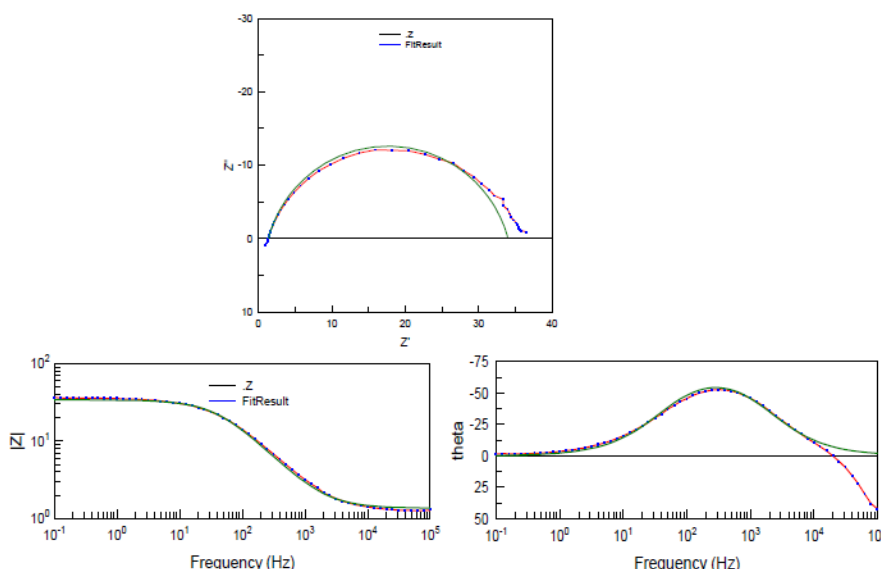


**Figure 10.** EIS Nyquist and Bode plots for carbon steel/1.0 M HCl interface: (dotted lines) experimental data; (dashed line) calculated.

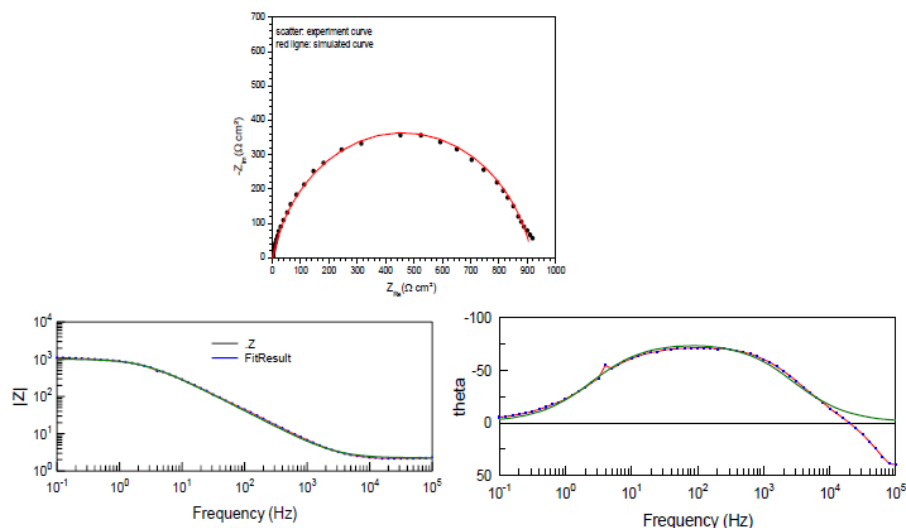


**Figure 11.** EIS Nyquist and Bode plots for carbon steel/1.0 M HCl with  $10^{-3}$  M M-QN interface: (dotted lines) experimental data; (dashed line) calculated.

**Table 5.** Electrochemical impedance parameters and inhibition efficiency for carbon steel in 1.0 M HCl solution without and with different concentrations of M-Qn at  $25 \pm 2$  °C.

Conc. of M-Qn (M)	$R_{ct}$ ( $\Omega \text{ cm}^2$ )	$C_{dl}$ ( $\mu\text{F cm}^{-2}$ )	n	$\eta_{EIS}$ (%)
Blank	35±1	298.0±4.0	0.79±0.02	-
$10^{-6}$	540±19	130.0±1.2	0.88±0.01	93.5
$10^{-5}$	611±26	120.0±1.7	0.86±0.01	94.2
$10^{-4}$	960±30	64.0±5.6	0.85±0.01	96.4
$10^{-3}$	1180±39	57.6±6.0	0.82±0.01	97.0

In Table 5 are also shown the calculated “double layer capacitance values ( $C_{dl}$ )”, and the relaxation time constant ( $\tau$ ) of charge-transfer process using the following equation (11):

$$\tau = C_{dl} R_{ct} \tag{11}$$

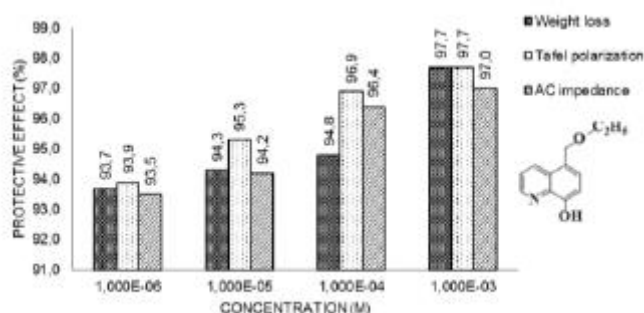


**Figure 12.** Inhibition efficiency values obtained from weight loss, Tafel polarization and AC impedance measurements of carbon steel in 1.0 M HCl at different concentrations of M-Qn at 25°C.

It is obvious from the results that M-Qn inhibited carbon steel corrosion in an 1.0 M HCl solution at its different concentrations, and  $\eta_{EIS}$  (%) was seen to continuously increase with the arise of concentration, reaching a maximum of 97.0 % at  $10^{-3}$  M. The inhibition efficiencies, calculated from Tafel impedance

results, showed the same trend as those obtained from EIS, polarization and weight loss measurements (Fig. 12).

### Effect of temperature

Temperature can modify the interaction between the carbon steel electrode and the acidic media without and with M-Qn. Thus, the potentiodynamic polarization curves for carbon steel in 1.0 M HCl in the absence and presence of  $10^{-3}$  M of M-Qn in the temperature range of  $25 \pm 2$  °C to  $55 \pm 2$  °C are shown in Figs. 13 and 14, respectively. It is remarked that these curves exhibited Tafel regions. It is also noted that the anodic and cathodic branches increased with the increase of temperature.

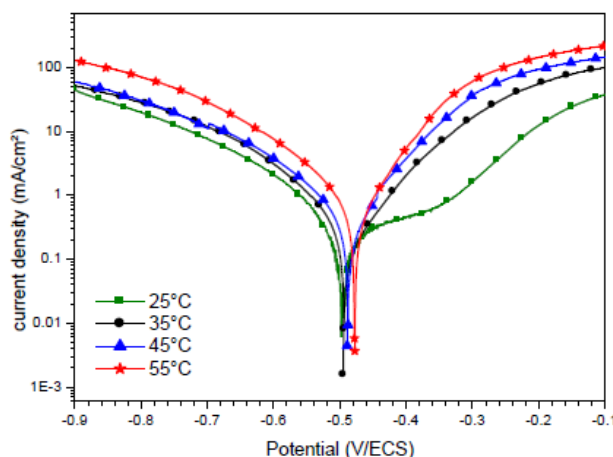


**Figure 13.** Potentiodynamic polarization curves for carbon steel in 1.0 M HCl in the absence of M-QN at different temperatures.

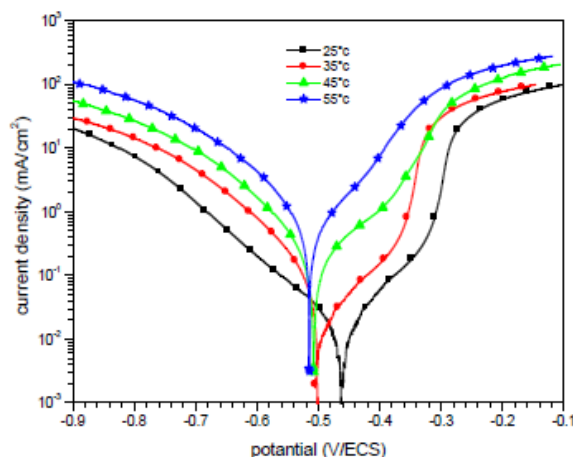


**Figure 14.** Potentiodynamic polarization curves for carbon steel in 1.0 M HCl in the presence of  $10^{-3}$  M of M-Qn at different temperatures.

The various electrochemical parameters were calculated from Tafel plots and are summarized in Table 6.

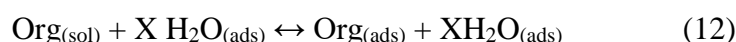
It can be seen that  $i_{corr}$  increased with an increase in temperature both in uninhibited and inhibited solutions, and the values of inhibition efficiency of M-Qn decreased with an increase in temperature. Thus, the inhibition efficiencies of M-Qn are temperature-dependent.

**Table 6.** Electrochemical parameters of carbon steel in 1.0 M HCl without and with  $10^{-3}$  M of M-Qn at different temperatures.

Compounds	Temp. °C	$-E_{\text{corr}}$ (mV/SCE)	$i_{\text{corr}}$ ( $\mu\text{A}/\text{cm}^2$ )	Tafel slops (mV/dec)		$\eta_{\text{pp}}$ (%)
				$-\beta_c$	$\beta_a$	
Blank solution	25±2	498	983	92	104	-
	35±2	491	1200	184	112	-
	45±2	475	1450	171	124	-
	55±2	465	2200	161	118	-
$10^{-3}$ M of M-Qn	25±2	453	22	125	84	97.7
	35±2	498	56	105	88	95.3
	45±2	504	158	98	93	89.1
	55±2	510	350	96	100	84.1

### Adsorption isotherm and thermodynamic parameters

The surface coverage values ( $\theta$ ) of carbon steel in 1.0 M HCl, in the presence of  $10^{-3}$  M of M-Qn, were obtained from weight loss measurements (Table 3). This parameter has been used to explain the best isotherm, in order to determine the adsorption process. As it is known, the adsorption of an organic adsorbate onto a metal/solution interface denotes a substitutive adsorption process between the organic molecules in the aqueous solution,  $\text{Org}_{(\text{sol})}$ , and the water molecules on the metallic surface,  $\text{H}_2\text{O}_{(\text{ads})}$  [42]:



where  $\text{Org}_{(\text{sol})}$  and  $\text{Org}_{(\text{ads})}$  are the organic molecules in the aqueous solution, and adsorbed onto the metallic surface, respectively,  $\text{H}_2\text{O}_{(\text{ads})}$  is the water molecules on the metallic surface, and X is the size ratio representing the number of water molecules replaced by one molecule of organic adsorbate [53].

However, the considered Langmuir isotherm model was as described in reference [54]:

$$\frac{\theta}{1-\theta} = K_{\text{ads}} \times C_{\text{inh}} \quad (13)$$

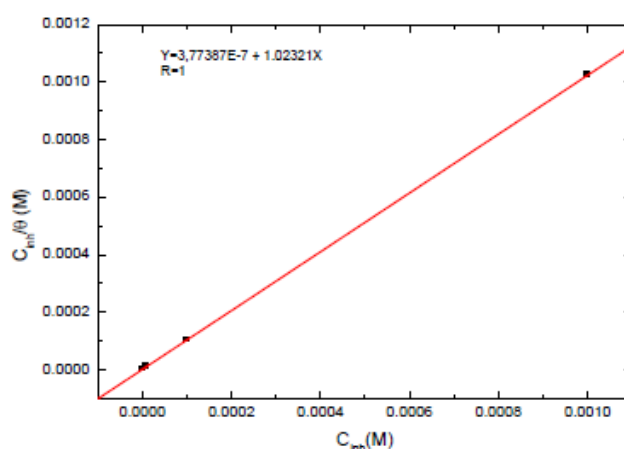


**Figure 15.** Plot of the Langmuir adsorption isotherm of M-Qn on the carbon steel surface at  $25 \pm 2$  °C.

In this study, the Langmuir isotherm was fitted. The best fit straight line (strong correlation with  $R^2 \approx 1$ ) is obtained for the plot of  $C_{inh}/\theta$  vs.  $C_{inh}$ , with slopes around unity (Fig. 15). This suggested that the adsorption of the studied inhibitor at the metallic surface obeyed Langmuir's adsorption isotherm model, and exhibited single-layer adsorption characteristics. This kind of isotherm involved the assumption of no interaction between the adsorbed species onto the electrode surface [55].

In addition, the adsorption constant,  $K_{ads}$ , was related to the free energy of adsorption,  $\Delta G_{ads}$ , by the following equation (14) [54]:

$$K_{ads} = \frac{1}{55.55} \exp\left(\frac{-\Delta G_{ads}^{\circ}}{RT}\right) \quad (14)$$

where 55.55 value represents the water concentration in solution by mol L<sup>-1</sup>, R is the universal gas constant and T is the absolute temperature.

The calculated value of the free energy of adsorption,  $\Delta G_{ads}$ , from the adsorption isotherm is -46.6 kJ mol<sup>-1</sup> at 25±2 °C. It is well known that values of  $\Delta G_{ads}$  of the order of -20 kJ/mol or lower indicate a physisorption; those of order of -40 kJ/mol or higher are associated with chemisorptions, as a result of the sharing or transfer of electrons from organic molecules to the metal surface, to form a coordinate; while values between -20 kJ mol<sup>-1</sup> and -40 kJ mol<sup>-1</sup> indicate both physisorption and chemisorption [41, 46, 48].

### Corrosion kinetic parameters

The data presented in Table 7 revealed that M-Qn took its inhibition efficiency at all temperature range.

**Table 7.** Values of activation parameters  $E_a$ ,  $\Delta H_a$  and  $\Delta S_a$  for carbon steel in 1.0 M HCl in the absence and presence of 10<sup>-3</sup> M of M-Qn.

Compounds	$E_a$ / kJ mol <sup>-1</sup>	$\Delta H_a$ / kJ mol <sup>-1</sup>	$\Delta S_a$ / J mol <sup>-1</sup> K <sup>-1</sup>
Blank solution	21.0	18.4	-126
10 <sup>-3</sup> M of M-Qn	76.0	73.3	140.3

This behavior confirmed the higher adsorption equilibrium constant  $K_{ads}$  values, indicating the physisorption and chemisorption of M-Qn at the carbon steel surface. This result has been explained by some authors as a likely specific interaction between the iron surface and the inhibitor. So, Ivanov [58] explained this increase in temperature by the change in the nature of the adsorption mode; the inhibitor is being physically adsorbed at lower temperatures, while this physisorption is favored by the increase in temperature. The same phenomenon was explained by other researchers as an increase in the surface coverage by the inhibitor [59]. Thus, at a surface with high coverage values, the diffusion through the surface layer containing the inhibitor and corrosion products became the rate-determining step of the metal dissolution process [60]. Thus, the inhibition properties of M-Qn can be explained by the kinetic model. The dependence of the corrosion value,  $i_{corr}$ , with the temperature can be regarded as an Arrhenius-type process given by equation (15) [61]:

$$\ln i_{corr} = \ln A - \frac{E_a}{RT} \quad (15)$$

where  $E_a$  is the apparent activation energy of the corrosion process,  $R$  is the universal gas constant,  $A$  is the Arrhenius pre-exponential constant and  $T$  is the absolute temperature.

The Arrhenius plots for carbon steel in 1.0 M HCl without and with  $10^{-3}$  M of M-Qn, according to equation (13), are presented in Fig. 16.

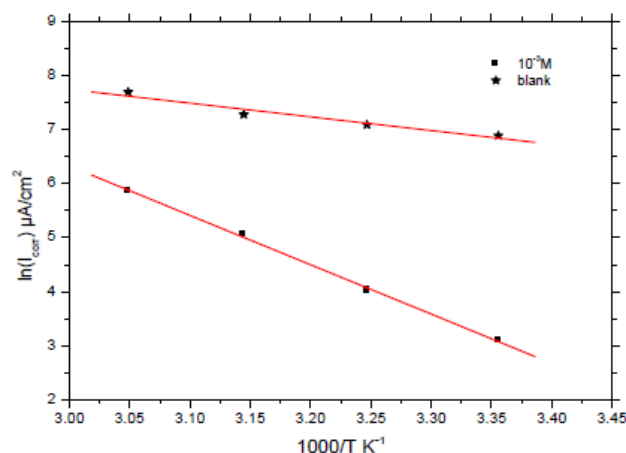


**Figure 16.** Arrhenius plots of carbon steel in 1.0 M HCl (a) without and (b) with  $10^{-3}$  M of M-Qn.

These obtained plots are straight lines, and the slope of each straight line gives the activation energy value,  $E_a$ . It is noted that the increase in the corrosion rate is more pronounced with the rise in temperature for the free solution. So, in the presence of M-Qn, the corrosion rate is slightly increased at explored temperatures. The  $E_a$  values were found to be equal to  $21.0 \text{ kJ mol}^{-1}$  and  $76.0 \text{ kJ mol}^{-1}$  in the absence and presence of  $10^{-3}$  M of M-Qn (Table 7).

The decrease of the inhibitor efficiency with an increased temperature, which referred to a higher value of  $E_a$ , when compared to the free solution, was interpreted as an indication of an electrostatic character of the inhibitor's adsorption. So, the investigated inhibitor significantly blocked some of the active sites on the metal surface. In general, the inhibitor adsorbed at the most active sites of the surface with lowest  $E_a$  and, thus, isolated them. Other active sites of higher  $E_a$  took part in the more intense corrosion process.

In addition, this change in  $E_a$  with the M-Qn addition can be attributed to the change in the corrosion process mechanism, in the presence of adsorbed inhibitor molecules [62].

Other kinetic data are accessible using the alternative formulation of the Arrhenius equation (16) [63]:

$$\ln \frac{i_{corr}}{T} = \ln \left( \frac{R}{Nh} \right) + \left( \frac{\Delta S_a}{R} \right) - \frac{\Delta H_a}{RT} \quad (16)$$

where  $h$  is Plank's constant,  $N$  is Avogadro's number,  $\Delta S_a$  is the entropy of activation and  $\Delta H_a$  is the enthalpy of activation.



Plots of  $\ln(i_{\text{corr}}/T)$  versus the reciprocal of temperature ( $1/T$ ) of carbon steel in 1.0 M HCl without and with  $10^{-3}$  M of M-Qn are presented in Fig. 17. Straight lines are obtained with a slope of  $\Delta H_a/R$  and an intercept of  $\ln R/Nh + \Delta S_a/R$ . The values of  $\Delta H_a$  and  $\Delta S_a$  are calculated and listed in Table 7. The positive sign of the enthalpies  $\Delta H_a$  improved the endothermic nature of the carbon steel dissolution process, whereas large negative values of entropies,  $\Delta S_a$ , implied that the activated complex in the rate determining step represents an association rather than a dissociation step, meaning that a decrease in disordering takes place on going from reactants to the activated complex [61-66].

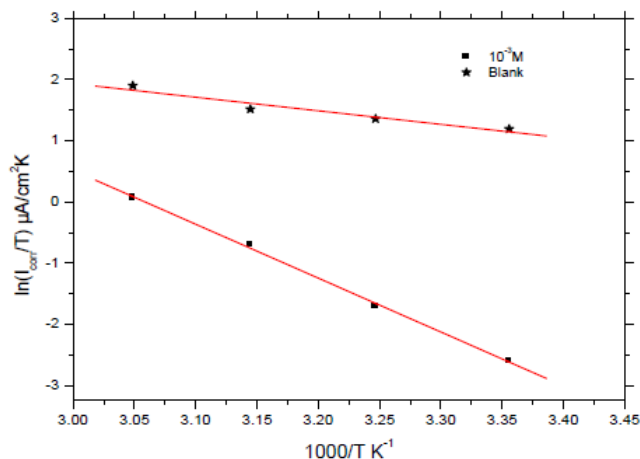


**Figure 17.** Transition-state plots for carbon steel in 1.0 M HCl (a) without and (b) with  $10^{-3}$  M of M-Qn.

## Conclusions

Concluding the experimental part, it was clearly demonstrated that all used techniques are able to characterize and follow the corrosion inhibition process promoted by 5-(ethoxymethyl)-8-quinolinol. The following conclusions can be drawn:

- The corrosion rate of carbon steel decreased with an increase in inhibitor's concentration, reaching a minimum at  $10^{-3}$  M.
- 5-(ethoxymethyl)-8-quinolinol exhibited good inhibition properties for carbon steel corrosion in 1.0 M HCl solution, and increased with an increase in the concentration of inhibitor.
- The obtained results showed that 5-(ethoxymethyl)-8-quinolinol acted as mixed-type inhibitor of carbon steel corrosion in 1.0 M HCl.
- EIS measurement results indicated that the resistance of the carbon steel electrode increased with inhibitor's concentrations, reaching a maximum at  $10^{-3}$  M of 5-(ethoxymethyl)-8-quinolinol.
- The inhibition efficiency of 5-(ethoxymethyl)-8-quinolinol can be stabilized by the participation of the two adsorption modes, physisorption and chemisorption.
- Thermodynamic adsorption parameters ( $\Delta H_a$ ,  $\Delta S_a$  and  $\Delta G_a$ ) showed that the studied inhibitor was adsorbed onto carbon steel surface by an endothermic and spontaneous process.

- Reasonably good agreement was observed between the obtained data from weight loss, potentiodynamic polarization curves and electrochemical impedance spectroscopy techniques.

## References

1. El Kacimi Y, Tourir R, Galai M, et al. *J Mater Environ. Sci.* 2016;7:371.
2. Hussin MH, Kassim MJ, Razali NN, et al. *Arab J. Chem.* 2011;1878.
3. Abbouda Y, Abourriche A, Saffaj T, et al. *Mater Chem Phys.* 2007;105:1.
4. James AO, Oforka NC, Abiola K. *Int J Electrochem Sci.* 2007;2:284.
5. Ebenso EE, Niger. *J Chem Res.* 2001;6:12.
6. Ekpe UJ, Okafor PC, Ebenso EE, et al. *Bull Electrochem.* 2001;17:135.
7. Alaoui K, El Kacimi Y, Galai M, et al. *J Mater Environ Sci.* 2016;7:2389.
8. Noor EA, Al-Moubaraki AH. *Int J Electrochem Sci.* 2008;3:806.
9. Alaoui K, El Kacimi Y, Galai M, et al. *Anal Bioanal Electrochem.* 2016;8:830.
10. Galai M, El Gouri M, Dagdag O, et al. *J Mater Environ Sci.* 2016;7:1562.
11. El Hezzat M, Assouag M, Zarrok H, et al. *Der Pharma Chemica.* 2015;7:77.
12. Obot IB, Obi-Egbedi NO. *Corros Sci.* 2009;52:276.
13. Obot IE, Obi-Egbedi NO. *Corros Sci.* 2010;52:657.
14. Ebenso EE, Alemu H, Umoren SA, et al. *Int J Electrochem Sci.* 2008;4:1325.
15. Abd El-Maksoud SA. *Appl Surf Sci.* 2003;206:129.
16. Hassan HH, Abdelghani E, Amina MA. *Electrochim. Acta.* 2007;52:6359.
17. Elkacimi Y, Achnin M, Aouine Y, et al. *Port Electrochim Acta.* 2012;30:53.
18. El Kacimi Y, Azaroual MA, Tourir R, et al. *Euro-Mediterr J Environ Integr.* 2017;2:1
19. Chetouani A, Hammouti B, Benhadda T, et al. *Appl Surf Sci.* 2005;249:375.
20. Khaled KF. *Mater Chem Phys.* 2008;112:290.
21. Chetouani A, Aounti A, Hammouti B, et al. *Corros Sci.* 2003;45:1675.
22. El Faydy M, Galai M, Tourir R, et al. *J Mater Environ Sci.* 2016;7:1406.
23. El Faydy M, Galai M, El Assyry A, et al. *J Molec Liq.* 2016;219:396.
24. Obot IB, Obi-Egbedi NO. *Corros Sci.* 2010;52:923.
25. Obot IB, Obi-Egbedi NO. *Mater Chem Phys.* 2010;122:325.
26. Watson AA, Fleet GWJ, Asano N, et al. *Phytochemistry.* 2001;56:265.
27. Abbouda Y, Abourriche A, Saffaj T, et al. *Mater Chem Phys.* 2007;105:1.
28. Xia Y, Yang ZY, Xia P, et al. *J Med Chem.* 1998;41:1155.
29. Chen YL, Chen IL, Tzeng CC, et al. *Helv Chim Acta.* 2000;83:989.
30. Peters W. *Chemotherapy and Drug Resistance in Malaria.* New York: Academic Press; 1970.
31. Sato M, Motomura T, Aramaki H. *J Med Chem.* 2006;49:1506.
32. Shukla SK, Quraishi MA. *J. Appl. Polym. Sci.* 2012;124:5130
33. Ashassi-Sarkhadi, Asghri E. *Electrochim. Acta.* 2008;54:162.

34. ASTM Practice Standard G-31, Standard Practice for Laboratory Immersion Corrosion Testing of Metals. West Conshohocken: ASTM International; 2004.
35. Stern M, Geary AL. *J Electrochem Soc.* 1957;104:56.
36. AbdelAal MS, Radwan S, El Saied A. *Br Corros J.* 1983;18:2.
37. El Faydy M, Galai M, El Assyry A, et al. *J Molec Liq.* 2016;219:396.
38. Williamson KL, Minard RD, Masters KM. *Macroscale and Microscale Organic Experiments.* 5th ed. 2007.
39. Hmamou DB, Salghi R, Zarrouk A, et al. *Ind Eng Chem Res.* 2013;52:14315.
40. Ateya BG, El-Khair MBA, Abdel-Hamed IA. *Corros Sci.* 1976;16:163.
41. Li W, He Q, Zhang S, et al. *J Appl Electrochem.* 2008;38:289.
42. Quraishi MA, Ahmad S, Venkatachari G. *Bull Electrochem.* 1996;12:109.
43. Riggs Jr OL. *Corrosion Inhibition.* 2nd ed. Houston: CC Nathan; 1973.
44. Ghareba S, Omanovic S. *Corros Sci.* 2010;52:2104.
45. Gerengi H, Darowicki K, Bereket G, et al. *Corros Sci.* 2009;51:2573.
46. Brug GJ, Van DenEeden ALG, Sluyters-Rehbach M, et al. *J Electroanal Chem.* 1984;176:275.
47. Moradi M, Duan J, Du X. *Corros Sci.* 2013;69:338.
48. Tang Y, Zhang F, Huc S, et al. *Corros Sci.* 2013;74:271.
49. Schultze JW, Wippermann K. *Electrochim Acta.* 1987;32:823.
50. Martinez S, Metikos M, Hukovic. *J Appl Electrochem.* 2003;33:137.
51. Hsu CH, Mansfeld F. *Corrosion.* 2001;57:747.
52. Khamis E. *Corrosion.* 1990;46:6.
53. Bentiss F, Lebrini M, Lagrenée M. *Corros Sci.* 2005;47:2915.
54. Adardour K, Kassou O, Tourir R, et al. *J Mater Environ Sci.* 2010;1:129.
55. Khaled KF. *Electrochim Acta.* 2008;55:3484.
56. Srhiri A, Etman M, Dabosi F. *Werkst Korros.* 1992;43:406.
57. Elayyachy M, El Idrissi A, Hammouti B. *Corros Sci.* 2006;48:2470.
58. Hongbo F. *Chem Industry Press.* 2002;166.
59. Ali SA, Al-Muallem HA, Saeed MT, et al. *Corros Sci.* 2008;50:664.
60. Popova A. *Corros Sci.* 2007;49:2144.
61. Raicheff R, Valcheva K, Lazarova E. in: *Proceeding of the Seventh European Symposium on Corrosion Inhibitors: Ferrara, Italy; 1990.* p 48.
62. Herrag L, Hammouti B, Elkadiri S, et al. *Corros Sci.* 2010;52:3042.
63. Marsh J. *Advanced Organic Chemistry.* 3rd ed. New Delhi: Wiley Eastern; 1988.
64. Martinez S, Stern I. *Appl Surf Sci.* 2002;199:83.
65. Galai M, El Gouri M, Dagdag O, et al. *J Chem Pharm Res.* 2015;7:712.
66. Dahmani M, Et-Touhami A, Al-Deyab SS, et al. *Int J Electrochem Sci.* 2010;5:1060.